Biosensors and Bioelectronics 146 (2019) 111741

Contents lists available at ScienceDirect

Biosensors and Bioelectronics

journal homepage: http://www.elsevier.com/locate/bios

Carbon dots-sensitized amorphous MoS_x photoanode: Sequential electrodeposition preparation and dual amplified photoelectrochemical aptasensing of adenosine

Yao Gao [a], Hui Qi [b], Mengxiang Shang [a], Jinling Zhang [a], Jianyue Yan [a], Wenbo Song [a,*]

[a] College of Chemistry, Jilin University, Changchun, 130012, PR China
[b] The Second Hospital of Jilin University, Changchun, 130041, PR China

ARTICLE INFO

Keywords:
Amorphous molybdenum sulfide
Carbon dots sensitization
Dual amplification
Sequential electrodeposition
Adenosine aptasensing

ABSTRACT

The design and fabrication of high visible-light activated photoelectrode are essential to precisely detect biomolecule in biological system. Herein, an ultrasensitive photoelectrochemical (PEC) aptasensor for specific recognition of adenosine is established based on carbon dots sensitized-amorphous molybdenum sulfide (a-MoS_x/CDs) photoanode and dual amplification strategy. The heterostructured photoanode achieved by sequential electrodeposition reveals significantly boosted photocurrent with good stability and repeatability under visible light illumination, giving the credit to highly activated visible light absorption, uniform coverage and good electric contact to the underlying substrate, as well as the energy-band alignment between the two components. By stepwisely immobilizing complementary DNA probe (NH_2-DNA) and adenosine aptamer (Apt), followed by methylene blue (MB) binding with the guanine base on Apt, a dual amplified self-powered PEC aptasensor for adenosine detection is constructed. Based on the co-sensitization effect of CDs and MB, ultrasensitive and high-affinitive determination of adenosine is realized over the concentration range of 0.01 nM–1000 nM at 0 V (vs. SCE), with satisfactory stability and reproducibility. The detection limit is as low as 3.3 pM, demonstrating a performance even surpassing most of the sensors reported so far. The prospective application of the co-sensitized a-MoS_x photoanode for ultrasensitive aptasensing is highlighted in this work.

1. Introduction

Adenosine is an endogenous nucleoside that performs an essential role in many different tissues and organs (Zhang et al., 2008). As a product of ATP degradation, adenosine has multiple information signal functions in both the peripheral and central nervous system. Numerous reports prove that excessive adenosine can suppress the immune response and promote malignancies growth (Giglioni et al., 2008; Spychala, 2000). It is therefore significant to monitor adenosine in biological systems for either biochemical study or clinical diagnosis.

Up to date, numerous methods have been developed for the identification and determination of adenosine, including capillary electrophoresis (Fang et al., 2013), thin layer chromatography (Akula et al., 2008), liquid chromatography (Capogrossi et al., 1982), mass spectrometry (Goodwin et al., 2019), colorimetry (Quan et al., 2015), surface enhanced Raman spectroscopy (Zhang et al., 2015), chemiluminescence (Yan et al., 2010), fluorescence (Hashemian et al., 2016) and electrochemistry (Wu et al., 2015). However, disadvantages exist including time consumption, complicated procedures, expensive instrumentation and poor repeatability. Recently, photoelectrochemical (PEC) biosensing has attracted considerable attention due to low background signal, ease of operation, high sensitivity and low cost (Dai et al., 2016; Wu et al., 2014; Zhou et al., 2016). The performance of a PEC sensor relies strongly on the properties of the photoactive materials (Xiong et al., 2018). As one of the recent fascinating photoactive materials, molybdenum disulfide (Shu et al., 2017), especially the electrodeposited amorphous molybdenum sulfide (a-MoS_x) is much attractive due to the ease of preparation, strong adhesion to underlying substrate, uniform coverage and excellent repeatability (Shang et al., 2018; Zhang et al., 2016). However, poor electron transport inhibits the PEC activity of a-MoS_x (Benck et al., 2012; Govindaraju et al., 2017). To modulate the PEC performance, formation of semiconductor heterostructure might be an efficient way (Han et al., 2018).

Because of notable optical and electric properties, carbon dots (CDs)

* Corresponding author.
E-mail address: wbsong@jlu.edu.cn (W. Song).

https://doi.org/10.1016/j.bios.2019.111741
Received 19 July 2019; Received in revised form 27 September 2019; Accepted 28 September 2019
Available online 28 September 2019
0956-5663/© 2019 Elsevier B.V. All rights reserved.

has been considered as a promising alternative to other nanocarbons (fullerenes, carbon nanotubes and nanodiamonds) and traditional toxic semiconductor quantum dots (CdS and CdSe QDs) in many applications (Baker and Baker, 2010; Wang et al., 2019). Particularly, CDs has an intrinsic band gap and exhibits outstanding PEC activity, contrary to the zero band gap graphene (Mao et al., 2019). Efficient photocatalytical removing complicated residual antibiotics has been reported by CDs/$BiVO_4$/Bi_3TaO_7 heterojunction (Le et al., 2019). Additionally, CDs normally acts as a sensitizer to improve the PEC property of some photoactive materials. Enhanced photocurrent density of WO_3 nanoplates by CDs sensitization is demonstrated based on energy-band alignment (Zhao et al., 2016). 7 folds increased photocurrent of ITO/-TiO_2 through CDs sensitization has been observed in a recent work from Cheng's group (Cheng et al., 2018).

Inspired by the ease of preparation, uniform coverage and excellent repeatability of the electrodeposited a-MoS_x, as well as the eco-friendly property, photo stability and low biological toxicity of the CDs, we herein design and fabricate a visible-light-activated a-MoS_x/CDs heterostructure with good electrical contact to the ITO substrate by sequential electrodeposition for adenosine aptasensing. By employing a-MoS_x/CDs hybrid films as photoactive matrix, the adenosine aptamer (Apt) probe is immobilized on the electrode surface via hybridization with the pre-anchored complementary DNA probe (NH_2-DNA). Methylene blue (MB) is subsequently attached on the Apt by virtue of the specific interaction with guanine base. When adenosine is incubated on the electrode, the MB-binding Apt would release from the electrode surface, resulting in photocurrent decrease based on the dual amplification strategy. The change in photocurrent enables ultrasensitive detection of adenosine quantitatively.

2. Experimental section

2.1. Preparation of a-MoS_x thin film

The ITO conductive glass sheets were cleaned with acetone, 0.1 M NaOH solution (ethanol: H_2O = 1:1; v/v) and ultrapure water for 15 min respectively, then dried at 60 °C for 12 h. The a-MoS_x film was prepared by electrochemical deposition according to the modified procedures in our previous work [18]. Briefly, the electrodeposition was carried out in a 2 mM $(NH_4)_2MoS_4$ aqueous solution using 0.1 M $NaClO_4$ as the supporting electrolyte in a three-electrode system with an ITO as the working electrode, a SCE and Pt plate as the reference and counter electrodes. The potential was scanned from -1.0 V to +0.5 V (vs. SCE) at a scan rate of 50 mV/s with the sweep segment of 30. The resultant ITO/a-MoS_x film was washed by ultrapure water and dried at 60 °C for 12 h under vacuum condition.

2.2. Fabrication of the a-MoS_x/CDs photoanodes

CDs was synthesized according to the previous report with minor changes (Guo et al., 2013) (with details shown in the Supporting Information). The CDs film was fabricated on the ITO/a-MoS_x surface by constant-voltage electrodeposition at +0.5 V (vs. Ag/AgCl) for 10 min in a two-electrode mode. The electrolyte was 0.1 mg/mL CDs solution. After deposition, the ITO/a-MoS_x/CDs films was thoroughly washed by ultrapure water and finally dried at 60 °C under vacuum condition.

2.3. Construction of PEC aptasensor

The procedures for the PEC sensor fabrication are illustrated in Scheme 1. Firstly, the chitosan (CS) solution (0.08 wt%) was prepared by dissolving CS powder in a 1% acetic acid solution. 20 μL of CS solution was coated on an ITO/a-MoS_x/CDs electrode. After drying at 50 °C, the electrode was washed with 0.1 M NaOH and ultrapure water several times. 20 μL of 5% glutaraldehyde (GLD) solution was dropped on the electrode. The electrode was kept at room temperature for 30 min and thoroughly rinsed with ultrapure water to remove physically adsorbed GLD. Then, by dropping 20 μL of 0.25 μM NH_2-DNA solution and incubating at 4 °C for 2 h, NH_2-DNA was introduced onto the GLD-activated electrode. To remove the unbounded NH_2-DNA, the electrode was thoroughly rinsed with 25 mM Tris-HCl buffer solution. 20 μL of 3% BSA solution was then cast onto the electrode and incubated for 1 h to block the unbound sites. After being rinsed with 25 mM Tris-HCl buffer solution, 20 μL of 0.25 μM Apt solution was cast onto the electrode surface. After incubating at 4 °C for 3.5 h, the electrode was rinsed with 25 mM Tris-HCl buffer solution. Finally, the electrode was coated with 20 μM MB solution and kept for 30 min at room temperature, followed by thoroughly rinsing with 10 mM Tris-HCl buffer solution (pH 7.4, 0.1 M NaCl, 10 mM KCl, and 10 mM $MgCl_2$). To assess the sensing performance, photocurrent measurement was performed at the proposed electrode that was incubated with adenosine solution of various concentrations at 37 °C for 1 h, followed by thoroughly washing with 10 mM PBS.

3. Results and discussion

3.1. Material characterization

The size of the synthesized CDs is characterized by HRTEM. As shown in Fig. S1, the prepared CDs have an average diameter of ~4 nm without apparent aggregation. Resolved lattice fringe with a lattice spacing of 0.32 nm, ascribed to the (002) facet of graphitic carbon, is observed in HRTEM image (inset of Fig. S1). The other physical properties of CDs are also investigated by UV–visible absorption spectroscopy and fluorescence spectroscopy. The UV–visible absorption spectrum of 0.1 mg/mL CDs aqueous solution is illustrated in Fig. S2A. The characteristic absorption peak locates at approximately 350 nm, attributed to the n–π* transition of C═O bond. The maximum fluorescence emission is found at 425 nm (Fig. S2B).

The photograph of electrodeposited a-MoS_x/CDs films on the ITO

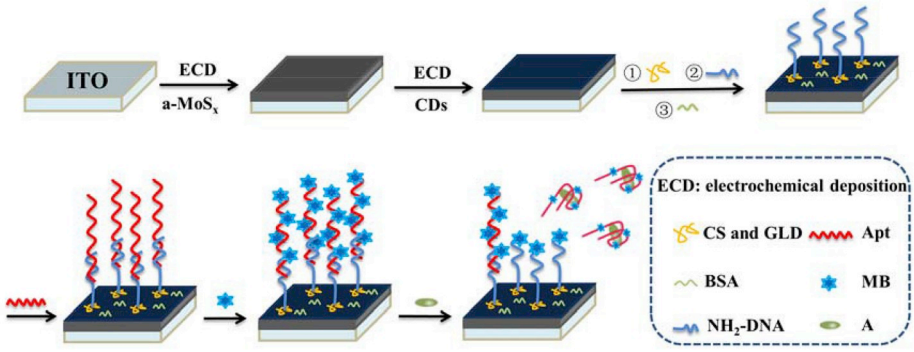

Scheme 1. Construction of the PEC aptasensor for detection of adenosine.

substrate is shown in Fig. 1A. One can see that the a-MoS_x/CDs heterostructured films is ultra-thin with good optical transparency. The morphology of a-MoS_x/CDs hybrid films is revealed by FESEM. The hybrid films is very flat and evenly covered the surface of ITO substrate without particle agglomeration (Fig. 1B). The chemical composition of a-MoS_x/CDs films was analyzed by X-ray photoelectron spectroscopy (XPS). Fig. 2A shows the Mo 3d spectrum that can be fitted into three doublet peaks. The doublet peaks at 228.1 eV (Mo $3d_{5/2}$) and 231.8 eV (Mo $3d_{3/2}$) are assigned to Mo^{4+} (Lu et al., 2016). The dominant peaks at 229.5 eV (Mo $3d_{5/2}$) and 233.1 eV (Mo $3d_{3/2}$) suggest the presence of Mo^{5+} (Merki et al., 2012). The binding energies of 232.4 eV (Mo $3d_{5/2}$) and 235.4 eV (Mo $3d_{3/2}$) are attributed to Mo^{6+} (Vrubel and Hu, 2013). Additionally, the peak of S 2s (226.2 eV) is also observed in Fig. 2A. Fig. 2B illustrates the fitted S 2p XPS spectra. The doublet peaks at 161.5 eV (S $2p_{3/2}$) and 162.7 eV (S $2p_{1/2}$) and the other doublet at 163.2 eV (S $2p_{3/2}$) and 164.3 eV (S $2p_{1/2}$) derive from S^{2-} ions (Chen et al., 2015) and bridging S_2^{2-} ligands (Kibsgaard et al., 2014), respectively. Above XPS analysis reveals that both Mo and S are multivalent states. Besides, the C 1s spectrum of a-MoS_x/CDs films is shown in Fig. 2C. Three characteristic peaks at 284.8, 286.3 and 288.6 eV are the signature of C–C, C–O/C–O–C and O═C–O bonding respectively (Ming et al., 2012; Zhao et al., 2016).

The comparable UV–visible absorption spectra of a-MoS_x and a-MoS_x/CDs films are presented in Fig. 2D. The heterostructured films exhibits stronger visible-light absorption than that of the a-MoS_x film, indicating that the CDs sensitization effect boosts the visible light absorption of a-MoS_x film. As can be seen from the inset in Fig. 2D and Fig. S2A, the band-gap energy (E_g) of a-MoS_x and CDs is ca. 1.81 eV and 2.03 eV, respectively.

3.2. PEC performance of a-MoS_x/CDs

The PEC response under visible light illumination was investigated. From Fig. 3A, the photocurrent of a-MoS_x/CDs is 14.34 nA, which is about two folds of the a-MoS_x (7.70 nA). The dramatic increase of photocurrent can be attributed to good visible light absorption of a-MoS_x/CDs. To highlight the importance of electrodeposition strategy, the CDs fabrication was also performed by immersing the ITO/a-MoS_x into 0.1 mg/mL CDs solution for 3 h. The photocurrent response at 0 V under visible illumination is compared in Fig. S3. The electrodeposition CDs generates a photocurrent nearly 1.5 times of that of dip coating CDs.

The Mott-Schottky (M-S) analysis was performed to measure the flat band potential values of a-MoS_x and CDs. In Fig. 3B and C, the slopes of the tangent lines are positive, indicating that both a-MoS_x and CDs are n-type materials. The flat band potential, determined by extrapolation to $C = 0$, is found to be -0.25 V vs. SCE (-0.01 V vs. NHE) and -0.49 V vs. SCE (-0.25 V vs. NHE) for a-MoS_x and CDs, respectively. Combining with the E_g of a-MoS_x and CDs (insets of 2D and 2E), the position of conduction band (CB) and valence band (VB) of a-MoS_x are -0.01 V (vs. NHE) and +1.80 V (vs. NHE), while the CB and VB of CDs are -0.25 V (vs. NHE) and +1.78 V (vs. NHE). Well-matched band alignment between a-MoS_x and CDs in the heterostructure is depicted Fig. 3D, ensuring facile electron-hole separation/transport and thereby boosting PEC response.

The effects of eletrodeposition parameter on the PEC response were investigated in detail. Fig. S4A depicts the a-MoS_x deposition cycle-dependent photocurrent. The electrodeposition was carried out with scanning the potential from -1.0 V to +0.5 V (vs. SCE) at a scan rate of 50 mV/s in a 2 mM $(NH_4)_2MoS_4$-containing electrolyte. As the deposition cycle increases from 5 to 15, the photocurrent enhances obviously. When the deposition exceeds 15 cycles, excessive a-MoS_x hinders electron transport and decreases the photocurrent. The influence of deposition time and CDs concentration in deposition solution on the photocurrent was also studied. In Fig. S4B, the photocurrent of a-MoS_x/CDs deposited in 0.1 mg/mL CDs solution is found to increase with deposition time from 5 min to 10 min. With further extending deposition time, the photocurrent decreases significantly. Fig. S4C illustrates the photocurrent change of a-MoS_x/CDs with the concentration of CDs deposition solution. When the CDs concentration varies from 0.05 to 0.1 mg/mL, the observed photocurrent increases gradually. It is reasonable that the more CDs deposited, the more enhancement in sensitization. The photocurrent begins to decrease as the CDs concentration exceeds 0.1 mg/mL, originating from the hindrance of electron transport from CDs agglomeration because of excessive deposition in high concentration solution (Fig. S4D).

3.3. PEC and EIS study on aptasensor construction

The stepwise construction process of the aptasensor was monitored by performing PEC measurements at 0 V under visible light illumination (Fig. 4A). The photocurrent of a-MoS_x/CDs is 14.34 nA (curve a). After immobilizing NH_2-DNA/BSA, the photocurrent intensity decreases dramatically (curve b), due to the block of interfacial electron transfer by non-conductive bioactive substances. The photocurrent further reduces after Apt hybridization. When MB specifically interacts with guanine base in the Apt, the photocurrent increases significantly (18.31 nA). As a well-known organic dye, MB possesses the good visible-light absorption (Fig. S5) and acts as an outstanding electron donor and photosensitizer in the visible region, benefiting to proliferated PEC response of a-MoS_x/CDs. After adenosine is captured by the Apt, the photocurrent intensity drastically decreases to 8.21 nA. Since the adenosine-binding Apt releases from the surface of electrode due to less stable of aptamer-DNA duplex compared with aptamer-analyte complex. Meanwhile, with the desorption of the Apt, the MBs are also released from the electrode surface, generating reduced photocurrent since the sensitization effect is weakened. The charge transport mechanism under visible light illumination is illustrated in Scheme S1. The photogenerated electrons generated from MB are transferred onto the conduction band (CB) of CDs. Owing to well-aligned band structures of a-MoS_x and CDs, the electrons are further transferred to the CB of a-MoS_x, finally to the ITO electrode. On the other hand, the remaining holes on

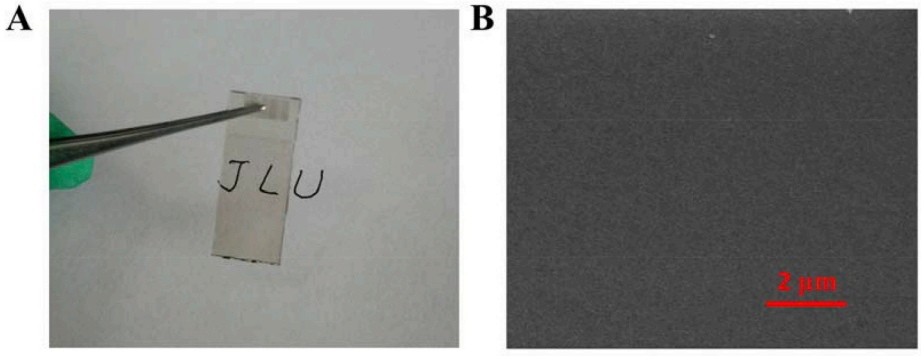

Fig. 1. (A) The photograph and (B) FESEM image of a-MoS_x/CDs hybrid films deposited on ITO substrate.

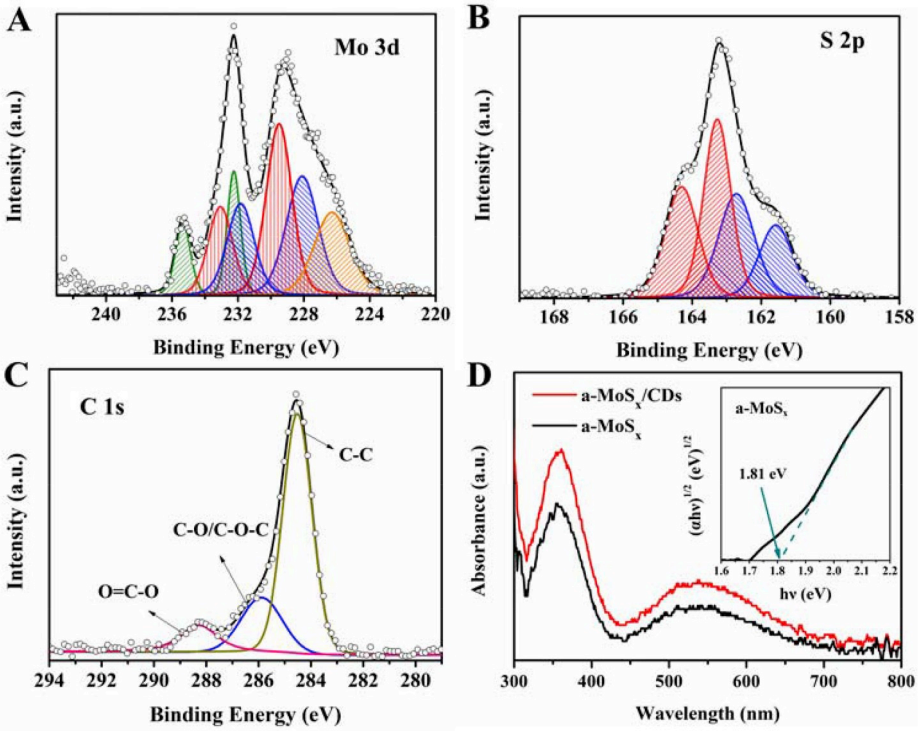

Fig. 2. High-resolution XPS spectra of (A) Mo 3d, (B) S 2p and (C) C 1s of a-MoS_x/CDs hybrid films. (D) UV–visible absorption spectra of a-MoS_x film and a-MoS_x/CDs hybrid films. The insets are related plots of $(\alpha h\nu)^{1/2}$ versus band-gap energy ($h\nu$).

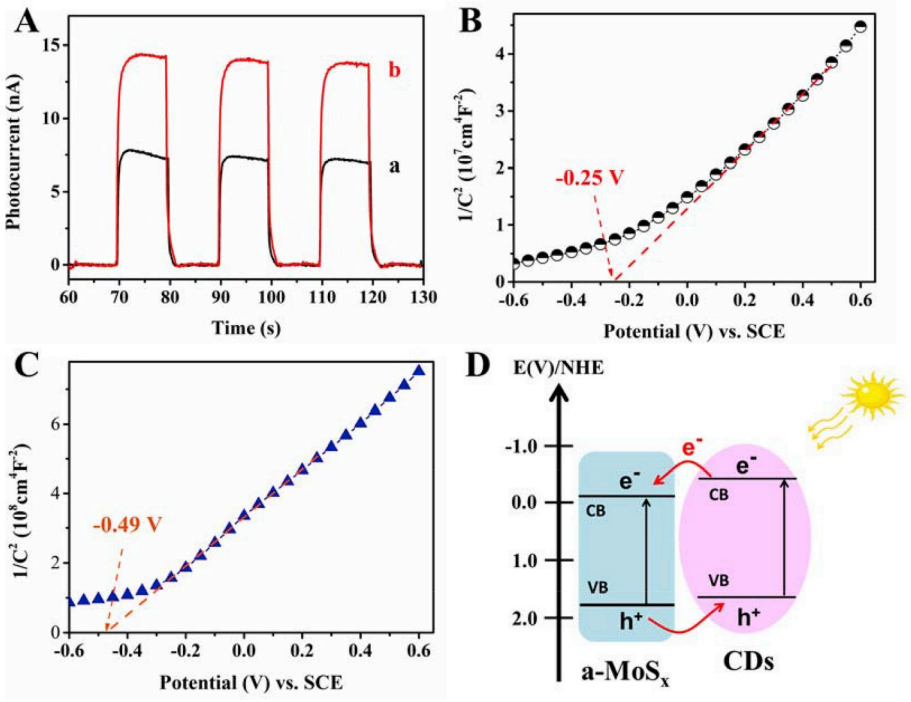

Fig. 3. (A) Comparative photocurrent responses of (a) ITO/a-MoS_x and (b) ITO/a-MoS_x/CDs. Mott-Schottky plots of (B) a-MoS_x and (C) CDs. (D) Illustration of the photo-generated charge transport through the heterostructure.

the valence band (VB) of a-MoS_x are first transferred to the VB of CDs. They are subsequently scavenged by electron donor, generating obvious photocurrent response.

Electrochemical impedance spectroscopy (EIS) is also involved to verify the successful construction of the PEC aptasensor. The diameter of the semicircle in EIS spectrum reflects the charge transfer resistance (R_{ct}) at the electrode/electrolyte interface. As shown in Fig. 4B, the a-MoS_x/CDs reveals a small semicircle diameter, indicating good conductivity (curve a). Sequential immobilization of the insulated proteins, NH_2-DNA/BSA and Apt, causes gradual increase of the semicircles (curve b and c). After the conductive MB was incubated to the Apt, significant decrease in the semicircle diameter is observed. Upon the

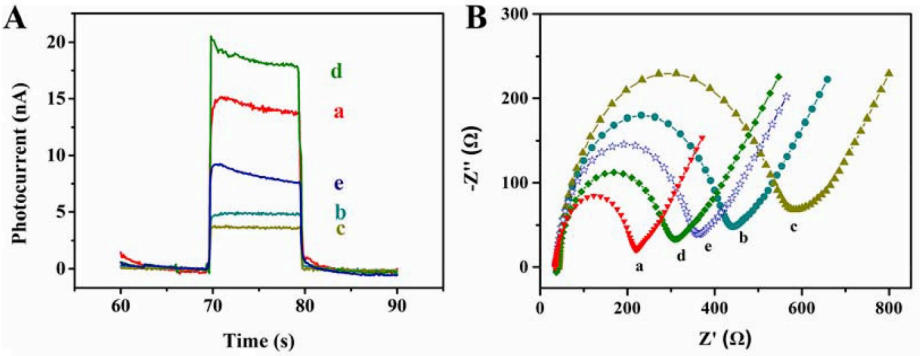

Fig. 4. (A) Photocurrent response and (B) electrochemical impedance spectra. (a) ITO/a-MoS_x/CDs, (b) ITO/a-MoS_x/CDs/NH_2-DNA/BSA, (c) ITO/a-MoS_x/CDs/NH_2-DNA/BSA/Apt, (d) ITO/a-MoS_x/CDs/NH_2-DNA/BSA/Apt/MB, (e) ITO/a-MoS_x/CDs/NH_2-DNA/BSA/Apt/MB/adenosine.

target recognition, the R_{ct} of the electrode begins to increase. Above EIS analysis agrees well with that of the PEC result. Both changes of the photocurrent and interfacial resistance reveal the successful fabrication of PEC sensor for adenosine detection.

3.4. Optimization of PEC aptasensor

In order to achieve optimal photocurrent for adenosine determination, some significant experimental factors for aptasensor construction were optimized. It is well-accepted that the maximum coating of Apt may not provide the greatest efficiency in affinity reaction due to steric hindrance. To optimize the Apt confinement and ensure high efficiency in the affinity reaction, the Apt concentration-dependent photocurrent of the sensor in the absence and presence of adenosine has been investigated, respectively. The related data (Fig. S7) and detailed discussions are provided in the Supplementary material. Based on the photocurrent change profile in Fig. S6A, one can see that the photocurrent of the aptasensor in the electrolyte containing 10 nM adenosine depresses quickly as the concentration of Apt increases from 0.1 to 0.25 μM. Upon the concentration exceeding 0.25 μM, the photocurrent intensity tends to stable. The optimal Apt concentration for fabricating the sensor is thus selected at 0.25 μM. Fig. S6B reveals the photocurrent change with the incubation time of Apt. With the increase in the incubation time from 2.5 to 3.5 h, the photocurrent intensity decreases dramatically. As the incubation time exceeds 3.5 h, the photocurrent tends to level off. Thus, the optimal incubation time is 3.5 h. Above optimization results indicate that, via incubation in 0.25 μM Apt solution for 3.5 h, the Apt immobilized on the electrode surface reaches saturation. Fig. S6C demonstrates that the concentration of MB greatly affects the photocurrent of the sensor. The intensity of photocurrent gradually increases with the concentration increase from 10 to 20 μM. When the MB concentration is more than 20 μM, the photocurrent keeps constant, suggesting that MB molecules on the Apt reach saturation. Therefore, 20 μM MB is adopted in the following experiments.

Under above optimal conditions, the effect of the incubation time between Apt and adenosine on the photocurrent was evaluated. It can be seen from Fig. S6D that the photocurrent gradually decreases with the increase of incubation time from 30 to 60 min. This is reasonable since the adenosine captured by Apt increases with time rising. Meanwhile, more MB molecules detach from the electrode surface as well. With the decrease of MB, sensitization effect is weakened, leading to a decrease in photocurrent. When the incubation time exceeds 60 min, the decrease of photocurrent is negligible, indicating that adenosine captured on the Apt reaches saturation. Therefore, the optimum incubation time is 60 min.

3.5. PEC detection of adenosine

Under the above optimal conditions, detection of adenosine was performed at 0 V under visible light illumination in 0.1 M PBS. The time-dependent current is found to decrease gradually with increasing adenosine concentration (Fig. 5A). Fig. 5B presents the linear-dependence of photocurrent to the logarithm of adenosine concentration in the range of 0.01–1000 nM. The linear equation can be expressed as I_{Photo} (nA) = -2.63$logC_{adenosine}$ (nM) + 11.35 (R^2 = 0.987). The detection limit is 3.3 pM (S/N = 3). Compared to the reported methods listed in Table S1, the proposed PEC aptasensor demonstrates a much lower detection limit with a broad linear range.

3.6. Selectivity, stability and reproducibility

To evaluate the selectivity of a-MoS_x/CDs/Apt/MB sensor for adenosine determination, the potential interferences including guanosine (G), uridine (U) and cytidine (C), were tested. Fig. 5C demonstrates that all these coexisting substances with 10-fold concentration do not induce any significant photocurrent signal, compared to adenosine under the same test conditions. The proposed PEC aptasensor is highly selective for adenosine. The stability evaluation of the aptasensor towards 1 nM adenosine was carried out by monitoring the photocurrent response in Fig. 5D. The photocurrent response retains 86.2% after 10 times on/off irradiation cycles.

The intraday precision was determined by repeating the analysis three times in a single day at the concentrations of 5 nM and 10 nM. Inter-day precision RSD was investigated for each day within 3 days. As shown in Table S2, the intraday RSD for 5 nM and 10 nM is 5.03% and 4.12%, respectively. The inter-day RSD for 5 nM and 10 nM is 4.57% and 3.89%. Both inter-day and intraday precisions are acceptable. Synchronously, no obvious photocurrent change is observed under 4 °C storage for 2 weeks, indicating a long-term storage stability of the proposed aptasensor. Employing five independently prepared a-MoS_x/CDs/Apt/MB electrodes, the RSD of photocurrent for 10 nM adenosine is 5.9%.

3.7. Analysis of real samples

To evaluate the applicability of the sensor for adenosine detection in real samples, the target detection was carried out in a serum sample diluted by 10 times with Tris-HCl buffer. As shown in Table S3, the concentration of adenosine in diluted serum sample is 7.16 nM. This value is consistent with the adenosine concentration quantified by HPLC (7.45 nM), demonstrating the reliability of the developed method. On the other hand, standard adenosine solution was added into the diluted human serum sample, which recovery was measured and summarized in Table S3. For the two spiked concentrations, the recoveries are in the range of 102.6–103.3% (RSDs within 3.4–3.8%). Above results indicate that the proposed sensor is applicable for real sample analysis.

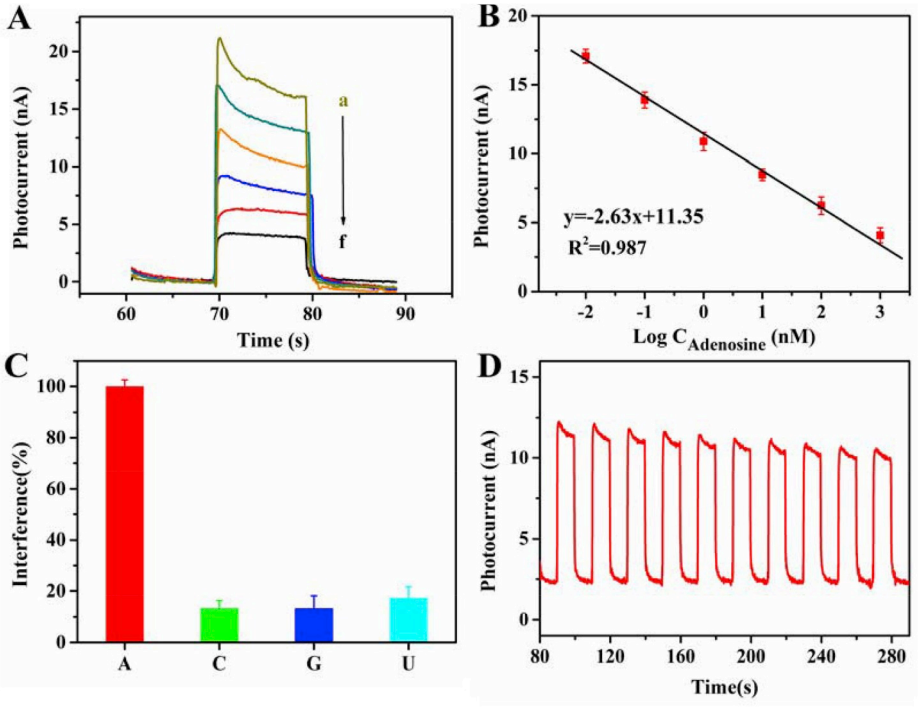

Fig. 5. (A) Photocurrent response to variable concentration of adenosine: (a) 0.01, (b) 0.1, (c) 1, (d) 10, (e) 100, (f) 1000 nM; (B) The corresponding calibration curve; (C) Selectivity of the sensor; (D) Stability test for 1 nM adenosine.

4. Conclusions

In summary, CDs sensitized-a-MoS_x heterostructured films with uniform coverage and good electric contact to the underlying ITO substrate has been achieved, which is directly used as visible-light-activated photoanode for self-powered PEC aptasensing of adenosine. By using CDs and MB as the photosensitizer and photoactive probe, dual amplification ensures ultrasensitive adenosine determination with a detection limit down to 3.3 pM, even outperforming most sensors reported so far. The highly selective signal-off PEC aptasensor is successfully applied to detect the target in serum samples at 0 V with desirable accuracy and satisfactory recovery. This work highlights the importance of sequentially electrodeposited a-MoS_x/CDs hybrid films with aligned energy-band structure for aptasensor fabrication and the reliability of co-sensitization effect on precise detection of biomolecules in biological systems. The proposed photoactive material and detection strategy may also pave the way for related biomedical research, disease treatment and clinical diagnosis.

Declaration of competing interest

The authors declare that they have no known competing financial interests or personal relationships that could have appeared to influence the work reported in this paper.

CRediT authorship contribution statement

Yao Gao: Investigation, Formal analysis, Writing - original draft. **Hui Qi:** Resources, Data curation. **Mengxiang Shang:** Methodology, Conceptualization, Writing - review & editing. **Jinling Zhang:** Writing - review & editing. **Jianyue Yan:** Visualization, Data curation. **Wenbo Song:** Supervision, Funding acquisition, Project administration.

Acknowledgment

This work was supported by the National Natural Science Foundation of China (No. 21874053 and No. 21475051); the Science and Technology Development project of Jilin province, China (No. 20180414022GH).

Appendix A. Supplementary data

Supplementary data to this article can be found online at https://doi.org/10.1016/j.bios.2019.111741.

References

Zhao, Z., Butburee, T., Peerakiatkhajohn, P., Lyu, M., Wang, S., Wang, L., Zheng, H., 2016. Chemistry 1 (11), 2772–2777.
Akula, K.K., Kaur, M., Kulkarni, S.K., 2008. J. Chromatogr. A 1209 (1), 230–237.
Baker, S.N., Baker, G.A., 2010. Angew. Chem. Int. Ed. 49 (38), 6726–6744.
Benck, J.D., Chen, Z., Kuritzky, L.Y., Forman, A.J., Jaramillo, T.F., 2012. ACS Catal. 2 (9), 1916–1923.
Capogrossi, M.C., Holdiness, M.R., Israili, Z.H., 1982. J. Chromatogr. B Biomed. Sci. Appl. 227 (1), 168–173.
Chen, Y., Tran, P.D., Boix, P., Ren, Y., Chiam, S.Y., Li, Z., Fu, K., Wong, L.H., Barber, J., 2015. ACS Nano 9 (4), 3829–3836.
Cheng, W., Pan, J., Yang, J., Zheng, Z., Lu, F., Chen, Y., Gao, W., 2018. Microchimica Acta 185 (5), 263.
Dai, H., Zhang, S., Hong, Z., Lin, Y., 2016. Anal. Chem. 88 (19), 9532–9538.
Fang, H., Pajski, M.L., Ross, A.E., Venton, B.J., 2013. Analytical Methods 5 (11), 2704–2711.
Giglioni, S., Leoncini, R., Aceto, E., Chessa, A., Civitelli, S., Bernini, A., Tanzini, G., Carraro, F., Pucci, A., Vannoni, D., 2008. Nucleosides Nucleotides Nucleic Acids 27 (6–7), 750–754.
Goodwin, K.J., Gangl, E., Sarkar, U., Pop-Damkov, P., Jones, N., Borodovsky, A., Woessner, R., Fretland, A.J., 2019. Anal. Biochem. 568, 78–88.
Govindaraju, G.V., Wheeler, G.P., Lee, D., Choi, K.-S., 2017. Chem. Mater. 29 (1), 355–370.
Guo, Y., Wang, Z., Shao, H., Jiang, X., 2013. Carbon 52, 583–589.
Han, Q., Wang, R., Xing, B., Chi, H., Wu, D., Wei, Q., 2018. Biosens. Bioelectron. 106, 7–13.
Hashemian, Z., Khayamian, T., Saraji, M., Shirani, M.P., 2016. Biosens. Bioelectron. 79, 334–340.
Kibsgaard, J., Jaramillo, T.F., Besenbacher, F., 2014. Nat. Chem. 6, 248.
Le, S., Li, W., Wang, Y., Jiang, X., Yang, X., Wang, X., 2019. J. Hazard Mater. 376, 1–11.
Lu, A.-Y., Yang, X., Tseng, C.-C., Min, S., Lin, S.-H., Hsu, C.-L., Li, H., Idriss, H., Kuo, J.-L., Huang, K.-W., Li, L.-J., 2016. Small 12 (40), 5530–5537.
Mao, L., Wang, X., Guo, Y., Yao, L., Xue, X., Wang, H.-X., Xiong, C., Wen, W., Zhang, X., Wang, S., 2019. Nanoscale 11 (16), 7885–7892.

Merki, D., Vrubel, H., Rovelli, L., Fierro, S., Hu, X., 2012. Chem. Sci. 3 (8), 2515–2525.
Ming, H., Ma, Z., Liu, Y., Pan, K., Yu, H., Wang, F., Kang, Z., 2012. Dalton Trans. 41 (31), 9526–9531.
Quan, K., Huang, J., Yang, X., Yang, Y., Ying, L., Wang, H., He, Y., Wang, K., 2015. Chem. Commun. 51 (5), 937–940.
Shang, M., Qi, H., Du, C., Huang, H., Wu, S., Zhang, J., Song, W., 2018. Sens. Actuators B Chem. 266, 71–79.
Shu, Y., Chen, J., Xu, Q., Wei, Z., Liu, F., Lu, R., Xu, S., Hu, X., 2017. J. Mater. Chem. B 5 (7), 1446–1453.
Spychala, J., 2000. Pharmacol. Ther. 87 (2), 161–173.
Vrubel, H., Hu, X., 2013. ACS Catal. 3 (9), 2002–2011.
Wang, M., Yin, H., Zhou, Y., Meng, X., Waterhouse, G.I.N., Ai, S., 2019. Chem. Eng. J. 365, 351–357.
Wu, S., Song, H., Song, J., He, C., Ni, J., Zhao, Y., Wang, X., 2014. Anal. Chem. 86 (12), 5922–5928.
Wu, D., Ren, X., Hu, L., Fan, D., Zheng, Y., Wei, Q., 2015. Biosens. Bioelectron. 74, 391–397.
Xiong, E., Yan, X., Zhang, X., Li, Y., Yang, R., Meng, L., Chen, J., 2018. Analyst 143 (12), 2799–2806.
Yan, X., Cao, Z., Lau, C., Lu, J., 2010. Analyst 135 (9), 2400–2407.
Zhang, S., Xia, J., Li, X., 2008. Anal. Chem. 80 (22), 8382–8388.
Zhang, C., Man, B.Y., Jiang, S.Z., Yang, C., Liu, M., Chen, C.S., Xu, S.C., Qiu, H.W., Li, Z., 2015. Appl. Surf. Sci. 347, 668–672.
Zhang, X., Li, L., Guo, Y., Liu, D., You, T., 2016. J. Colloid Interface Sci. 472, 69–75.
Zhao, S., Li, C., Wang, L., Liu, N., Qiao, S., Liu, B., Huang, H., Liu, Y., Kang, Z., 2016. Carbon 99, 599–606.
Zhou, L., Jiang, D., Du, X., Chen, D., Qian, J., Liu, Q., Hao, N., Wang, K., 2016. J. Mater. Chem. B 4 (37), 6249–6257.